IOSR Journal of Applied Chemistry (IOSR-JAC)
ISSN: 2278-5736. Volume 3, Issue 3 (Jan. – Feb. 2013), PP 45-53
www.iosrjournals.org

Deactivation of photocatalytically active ZnO nanoparticle by surface capping with poly vinyl pyrrolidone.

M. Sudha[1], M. Rajarajan[2*]
[1]*Department of Chemistry, Nadar Saraswathi College of Engineering & Technology,Theni – 625 531.*
[2]*P.G. Department of Chemistry, Cardamom Planters' Association College, Bodinayakanur – 625 513.*

Abstract: *Nanoparticles of zinc oxide (ZnO) were prepared by the precipitation method from zinc sulphate ($ZnSO_4.7H_2O$) and sodium bicarbonate ($NaHCO_3$). Organization, stabilization of the ZnO nanoparticles from further growth and partially inhibiting the photodegradation was achieved by capping with poly vinyl pyrrolidone (PVP). Fourier transform infrared spectroscopy (FTIR), X-ray powder diffraction (XRD), scanning electron microscopy (SEM) and transmission electron microscopy (TEM) were used to investigate the structure, morphology and particle size. Thermogravimetric-differential thermal analysis (TG-DTA) was used to study the thermal behavior. In addition, photocatalytic degradation of Rhodamine B (RhB) in aqueous solution was performed using bare and modified ZnO nanoparticles under the illumination of UV light. Various parameters affecting the degradation performance such as catalyst loading, initial dye concentrations, pH and concentration of capping agent were examined. The results showed that PVP capped ZnO nanoparticles have reduced photocatalytic activity than that of bare ZnO nanoparticles. The reduction in the chemical oxygen demand (COD) and total organic carbon (TOC) results revealed the reduced photocatalytic activity of PVP capped ZnO. The UV-shielding property was evaluated by measuring the transmittance. The reduced photocatalytic activity of PVP capped ZnO nanoparticles will enhance their performance as durable, safe and non reactive UV blockers in cosmetics.*

Keywords*: Photocatalysis, ZnO nanoparticles, Polymer capping, Dye degradation, Rhodamine B.*

I. Introduction

Over the years, a large number of semiconductors have been used as photocatalysts. The most commonly studied photocatalysts are TiO_2 and ZnO [1]. As a semiconductor oxide, TiO_2 has been investigated extensively since 1980s and found as a photocatalyst due to its abundant availability and chemical stability [2]. However, widespread use of TiO_2 is uneconomical for large scale and it has become an imperative to find a suitable alternative. Some studies have confirmed that ZnO can also be used as a very efficient photocatalyst [3, 4]. ZnO is of lower cost and exhibits higher photocatalytic efficiencies for the degradation of several organic pollutants, such as some dyes, in both acidic and basic medium than TiO_2 [5, 6]. Therefore, ZnO has been found to be a suitable alternative to TiO_2.

ZnO is one of the most important n-type semiconductor materials with a 3.37 eV band gap at room temperature and 60meV excitation banding energy [7] that is in the UV region and makes this nanoparticle as an efficient UV absorber [8,9]. It also shows remarkable potential application in catalysts [10], electrical and optical devices [11], varistors [12], gas sensors [13, 14], solar cells [15], cosmetic materials and so on. In addition, ZnO is nontoxic and environmentally friendly that is valuable for bio-applications [16].

Zinc oxide is a material with many important and diverse applications. Approximately, 45% of the world year production of ZnO is used in the rubber industry to control the vulcanization process and as additive [17]. In the methanol synthetic process ZnO is part of the Cu, ZnO, Al_2O_3 catalyst [18]. In the pharmaceutical industry ZnO is applied in ointments because of its antiseptic properties [18]. The optical properties make ZnO also suitable for many applications, like as pigment in paints, as UV filter in products for sun protection and for the production of LEDs and TFTs [19]. For this wide range of applications ZnO is used often in the form of particles and the size of the particles plays an important role.

Because ZnO can absorb the UV part of solar light, it has been widely used as an excellent UV absorber in outdoor textile and cosmetics products [20, 21]. Ultrafine ZnO particles show a high degree of transparency due to their negligible light scattering power [22, 23] making ZnO useful in sunscreen, paints, varnishes and plastics applications. However, the application of ZnO as a UV absorber is limited in practical areas because of the inherent photocatalytic activity of ZnO. When the irradiation energy exceeds the band gap energy of ZnO, electron-hole pairs will be generated. The photo generated charges cause oxidation reactions on the particle surface, giving rise to free radicals which in turn degrade organic molecules, resulting in color fading of fabric [24,25] and damage of the skin cells [26]. Hence in order to utilize ZnO nanoparticles as UV absorbers in a safe and effective manner, it is of particular importance to develop the methods to reduce the photocatalytic activity of ZnO. One of the approaches to reduce the photocatalytic activity of ZnO is to build a

barrier between ZnO and the surrounding material to prevent direct contact between them by means of surface modification.

Numerous modification methods are found in the literature, which are aimed at preventing particle growth. Lot of publications report on the stabilization of ZnO with different polymers: PEI [27] and polyvinylpyrrolidone (PVP) [28-31] are most widely used. Polyvinylpyrrolidone (PVP-K30) is water-soluble, low-cost, environmentally friendly and commonly used in food processing. Recently, PVP-K30 has been successfully used as the capping molecules to synthesize highly monodisperse wurtzite ZnO nanoparticles and the sterically stabilized PVP-silver nanoparticles (PVP-AgNPs) [32, 33].

In the present investigation with the aim to reduce the photocatalytic activity of ZnO nanoparticles and to improve its UV blocking property PVP is used to modify the surface of ZnO nanoparticles.

II. Experimental

All chemicals were of analytical grade, purchased from SD fine chemicals and were used without any further purification

2.1. Synthesis

2.1.1. Synthesis of ZnO nanoparticles

ZnO nanoparticles were synthesized according to the procedure described by ChangChun Chen et al. [34]. In a typical synthesis of bare ZnO nanoparticles 4.16 g of $ZnSO_4.7H_2O$ (0.1M) and 3.36g of $NaHCO_3$ (0.2M), each portion was separately dissolved in 200 ml of distilled water. Then $NaHCO_3$ solution was added dropwise into $ZnSO_4.7H_2O$ solution with constant stirring using magnetic stirrer. And then, the precipitates derived from the reaction between the $ZnSO_4.7H_2O$ and $NaHCO_3$ solutions were collected by filtration and rinsed three times with distilled water and ethanol. Subsequently, the washed precipitates were dried at 80°C to form the precursors of ZnO. Finally, the precursors were calcined at a temperature of 350°C for 3 h in the muffle furnace to obtain the nano-sized ZnO particles.

2.1. 2. Synthesis of PVP capped ZnO nanoparticles

First, $ZnSO_4.7H_2O$ (1M) was dissolved in distilled water. Then PVP solution was prepared by dissolving 100mg in 20 ml distilled water and was added to $ZnSO_4.7H_2O$ solution. $NaHCO_3$ (2M) was prepared separately and was added dropwise in to the above $ZnSO_4$ solution under constant stirring to form PVP capped ZnO nanoparticles. The solution mixture was then stirred continuously at room temperature for upto 2 hrs and allowed to settle. The precipitates formed were then filtered, washed, dried at 80°C and calcined at 350°C to get PVP capped ZnO nanoparticles.

2.2. Characterization of ZnO nanoparticles

The bare and the PVA capped ZnO nanoparticles were characterized by X-ray powder diffraction (XRD) using Analytical X per PRO X-ray diffractometer with CuKα radiation. The IR spectral data were obtained between the wave number of 400 and 4000 cm^{-1} using Perkin Elmer FT-IR spectrophotometer 1725x. Scanning electron microscope (SEM) images were obtained using HITACHI model S-3000H. The morphology of the bare and the PVA capped ZnO nanoparticles were determined by transmission electron microscope (TEM) using FEI Tecnai G2 20 S -TWIN high resolution transmission electron microscope. The thermal behavior was studied using thermogravimetric – differential thermal analysis at 10 °$Cmin^{-1}$ heating rate.

2.3. Photocatalytic activity test

Rhodamine B (RhB) was used as a probe molecule to evaluate the photocatalytic activity of bare and PVA capped ZnO nanoparticles in response to UV light irradiation. The characteristic optical absorption peak of RhB at 554 nm was chosen to monitor the photocatalytic degradation process. The experiment was carried out in a HEBER IMMERSION TYPE photoreactor (HIPR - Compact - p -8/125/250/400) and pH was adjusted using EUTECH instrument pH meter.

100 ml of aqueous 10^{-5} M RhB solution was taken in the cylindrical glass vessel with a circulating water jacket to maintain constant temperature, in which air was bubbling continuously from the bottom of the reactor. Then, bare ZnO nanoparticles were added into the vessel. Before irradiation, the aqueous suspensions containing dye solution and catalyst were continuously stirred for 30 min in dark to reach an adsorption-desorption equilibrium. After that, the mixture was subjected to UV irradiation. At regular intervals, 5 ml of the aliquot samples were withdrawn from the reaction mixture and centrifuged at 4000 rpm for 20 min to separate the nanoparticles. A JASCO V-530 UV/VIS spectrophotometer was used to follow the disappearance of RhB in the degraded solution. The procedure was repeated with PVP capped ZnO nanoparticles also.

Two control experiments were also conducted to test: (1) the adsorption of dye on the ZnO nanoparticles in darkness and (2) photodegradation of the dye when exposed to UV light without the catalyst ZnO.

COD was estimated before and after the treatment using $K_2Cr_2O_7$ oxidation method. The photodegradation efficiency was calculated according to Eq. (1).

$$\text{Photodegradation efficiency} = \frac{\text{Initial COD} - \text{Final COD}}{\text{Initial COD}} \times 100 \quad \ldots\ldots \text{Eq. (1).}$$

The extent of photodegradation of RhB was also measured using total organic carbon analyzer (Shimadzu TOC –V CPN).

2.4. Evaluation of UV shielding property

The UV-shielding property of the particle was evaluated by measuring the transmittance of the film consisting of uniformly dispersed sample powder with a UV-Vis spectrophotometer (JASCO V-530), where 2 g of sample powder, 4 g of industrial grade nitrocellulose, 10 g of ethyl acetate and 9 g of butyl acetate were mixed uniformly using paint shaker and 100 g of zirconia ball (2.7 mm in diameter) for 24 h. The dispersion mixture was applied onto a quartz glass plate with an applicator. Thickness of the film was 3 μm after drying at room temperature for 24 h.

III. Results and discussion

3.1. Characteristics of ZnO and PVA capped ZnO nanoparticles

3.1.1 X-ray diffraction

Fig.1. illustrates the XRD spectra of ZnO nanoparticles before and after PVP capping. Fig.1a shows the XRD spectra of bare ZnO nanoparticles in which all peaks can be well indexed to the wurtzite phase of ZnO (International standard for diffraction Data, JCDPS 36-1451). No peaks from other phase of ZnO and impurities are observed, suggesting that high purity of ZnO be obtained. These peaks are broad, suggesting that the crystallites have sizes in the nanometer range and the diameter D was calculated using Debye-Scherrer formula $D = K\lambda/(\beta\cos\theta)$, where K is the scherrer constant, λ the X-ray wavelength, β the peak width of half maximum, and θ is the Bragg diffraction angle.

The broad diffraction peaks of the sample after capping shown in Fig.1b confirmed that the crystal structure of ZnO nanoparticles was not altered during the capping process. The XRD peaks give the diameter of about 25 nm for bare and about 15 nm for PVP capped ZnO nanoparticles.

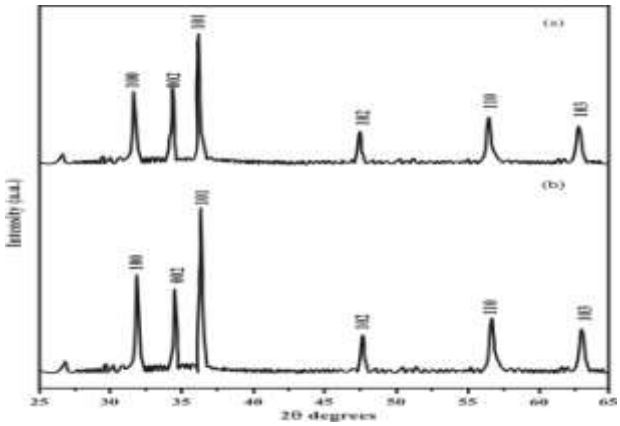

Fig. 1. XRD pattern of bare and PVP capped ZnO nanoparticles.

3.1.2. FT-IR spectra

Fig.2. shows the FT-IR spectra of both bare and modified ZnO nanoparticles. In the FT-IR spectra of bare ZnO nanoparticles (Fig.2a), the peak at 463cm^{-1} is the characteristic absorption of Zn-O bond and the broad absorption peak at 3438cm^{-1} can be attributed to the characteristic absorption of hydroxyls.

In the FT-IR spectrum of PVP capped ZnO nanoparticles (Fig.2b), several peaks are shown at 3414, 1646 and 1375, 1200,509 and 425 cm^{-1}. The observed peak at 1646 cm^{-1} is a distinct stretching mode of carbonyl group on the PVP molecule and the peak at 1375 cm^{-1} is due to the bending mode of CH_2 while the peak at 1200 cm^{-1} results from the stretching mode of C-N in PVP molecule. The PVP capping of ZnO

nanoparticles is confirmed through FT-IR spectroscopy, which suggests that a monomolecular layer on ZnO nanoparticles surface be formed.

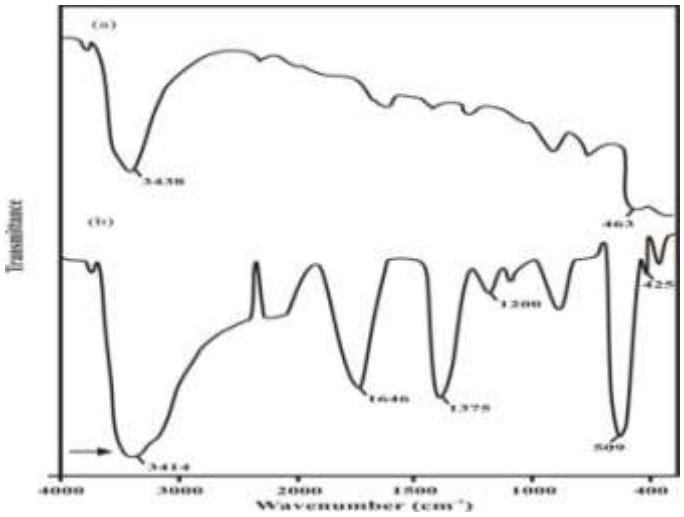

Fig.2. FT-IR spectra of bare and PVP capped ZnO nanoparticles

3.1.3. Scanning electron microscope

The SEM images of bare and PVP capped ZnO nanoparticles are shown in Fig.3a and b which shows that the bare ZnO nanoparticles are needle shaped with particle size of 20 - 30 nm which is in line with the results from XRD while the PVP capped ZnO nanoparticles were obtained as nanospheres with particle size of 10 -20 nm which proves the role of polymer capping in the size and morphology of ZnO nanoparticles.

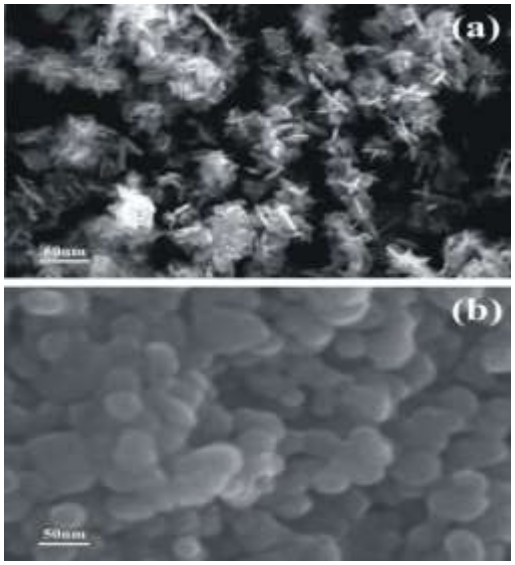

Fig. 3. SEM images of bare and PVP capped ZnO nanoparticles

3.1.4. Transmission electron microscope

Fig.4. illustrates the TEM images of bare and PVP capped ZnO nanoparticles. Fig.4a shows the TEM image of bare ZnO nanoparticles that was synthesized by precipitation method which consists of well dispersed needle shaped single crystal particles with a reasonably narrow size distribution and their diameter is about 25 nm. This result is in accordance with the value calculated from the X-ray diffraction.

Fig.4b shows the TEM image of PVP capped ZnO nanoparticles, in which physical separation of the particles was maintained during processing, thus preventing the formation of agglomerates. Besides, one can also observe that around the ZnO nanospheres there encircle some shadows, implying the existence of capped PVP. This is due to the fact that PVP can form a shell surrounding the particles to prevent them from being large in size by means of aggregation.

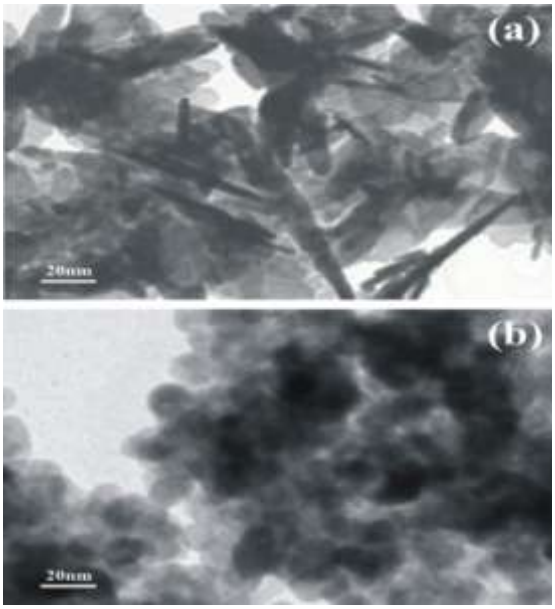

Fig. 4. TEM images of bare and PVP capped ZnO nanoparticles

3.1.5. Thermogravimetric-differential thermal analysis (TG-DTA)

To further confirm the interactions between PVP and ZnO nanoparticles the thermal behavior of the PVP capped ZnO nanoparticles was investigated. Fig.5. shows the TG-DTA curves of the as derived material after washing, before thermal treatment. The TGA curve exhibits three apparent mass losses, the first one between 50 – 150^{0}C is due to the loss of residual solvent and water. The second and third mass loss observed in the region 380 - 450^{0}C and 450 -550^{0}C is due to the thermal decomposition of organics. The DTA curve shows three exothermic peaks around 410, 430 and 520^{0}C indicating that there might exist weak interactions between PVP and ZnO nanoparticles.

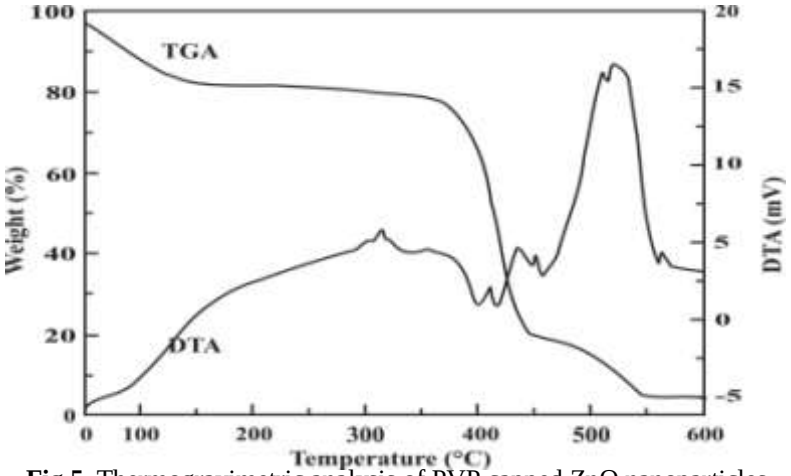

Fig.5. Thermogravimetric analysis of PVP capped ZnO nanoparticles

3.2. Photocatalytic activity

3.2.1. Optimal conditions for photocatalytic degradation

To select an appropriate condition for comparison of photocatalytic activity the optimum values of different parameters viz. catalyst dose, pH of the solution and initial concentration of the dye affecting the degradation efficiency of RhB were investigated. Initially blank experiments were performed under UV irradiation without addition of any catalyst and in darkness which shows negligible degradation.

Fig.6. justifies selection of appropriate conditions on the photocatalytic activity of bare ZnO nanoparticles. The results show that the increase of catalyst loading increases the degradation rate due to increase in the catalyst surface area, which enhances number of active sites. The constancy at higher catalyst loading beyond the optimum level of 0.5g shown in Fig 6a is due to decrease in light penetration and deactivation of activated molecules due to collision with the ground state molecules. Further at higher catalyst

loading it is difficult to maintain the suspension homogeneous due to particles agglomeration which decreases the number of active sites.

Fig. 6b shows the photodegradation efficiency of RhB as a function of pH. It has been observed that the degradation efficiency increases with increase in pH exhibiting maximum degradation efficiency at pH 8 beyond which the degradation was found to be decreased. The degradation was good and the enforcement of the reaction rate under alkaline conditions could be attributed to the increase of hydroxyl ions, which induces more hydroxyl radical formation. The formed •OH radicals initiate the degradation reaction.

Fig. 6c shows that the photocatalytic degradation efficiency was found to increase with increasing concentration of RhB upto $2x10^{-5}$M. On further increasing its concentration, a sudden decrease in the rate of degradation was observed. This may be explained on the basis that on increasing the concentration of RhB, more molecules of RhB are available for degradation. However on increasing the concentration above $2x10^{-5}$M, the reaction rate was found to decrease. It may be attributed to the fact that as the concentration of RhB was increased, it started acting as filter for the incident light, where its larger concentration will not permit the desired light intensity to reach the dye molecule in the bulk of the solution.

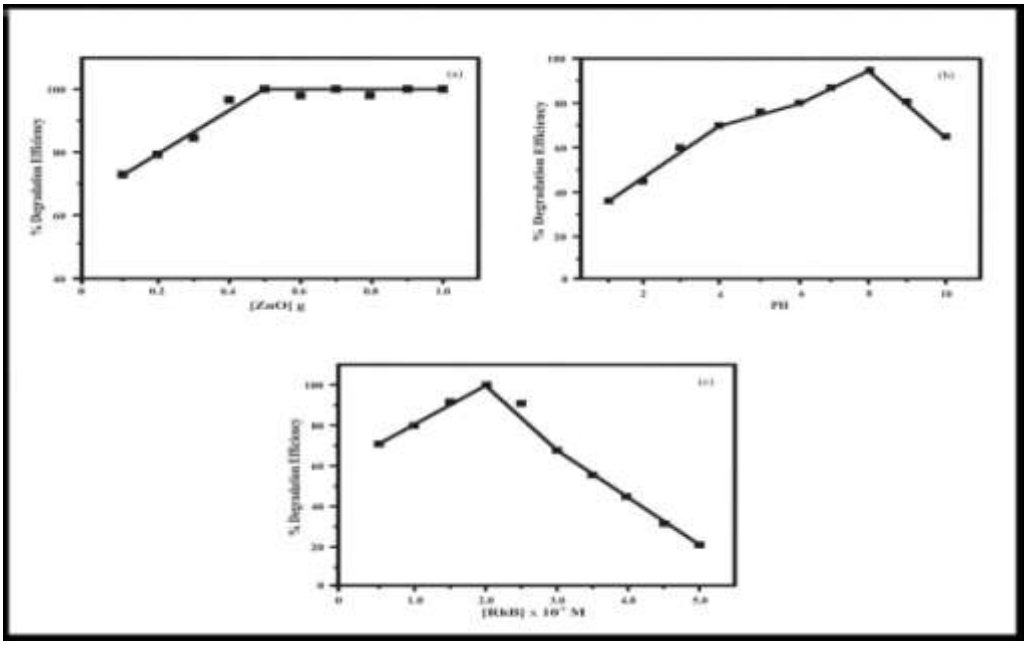

Fig. 6 a Effect of catalyst loading on the degradation efficiency of RhB, pH = 8, [RhB] = $2x10^{-5}$ M.

b Effect of pH on degradation efficiency of RhB, [RhB]=$2x10^{-5}$M, [ZnO]=0.5g.

c Effect of RhB concentration, pH = 8, [ZnO] = 0.5 g.

3.2.2. Comparison of Photocatalytic activity of bare and PVP capped ZnO nanoparticles

Bare and PVP capped ZnO nanoparticles were used as photocatalysts respectively to degrade RhB dissolved in water and the corresponding time dependent optical absorption spectra of RhB aqueous solutions under the irradiation of UV light are shown in Fig. 7. From Fig. 7a the UV absorption peaks of RhB became weaker as the irradiation time was prolonged and disappeared completely after 150 min under UV irradiation. It was also observed that no hypochromic shift and no new absorption peaks appeared during the irradiation which obviously indicates the absence of any intermediate formation. Hence, the total degradation of RhB occured via the cleavage of the chromophoric ring structure.

A similar trend was observed for PVP capped ZnO nanoparticles, as shown in Fig.7b. It could be seen that the bare ZnO nanoparticles have high photocatalytic activity while the activity was greatly reduced if the surface of ZnO nanoparticles was capped with PVP. This may be due to the fact that bare ZnO nanoparticles are hydrophilic. They can absorb more RhB molecules in water and can contact with air closely. While the PVP capped ZnO nanoparticles are hydrophobic leading to little photocatalytic activity. That is, the PVP coated on the surface of ZnO nanoparticles interfere with the absorption of the RhB molecules and the contact with air. The photocatalysis experiment also implied that a thin layer of PVP was formed on the surface of ZnO nanoparticles to reduce the photocatalytic property of ZnO nanoparticles. This agrees with the FT-IR analysis also. It can be easily understood that, the PVP on the particle surface does not possess photocatalytic capability and will not generate the couple of void and electron under UV irradiation. Although the inner of the nanoparticles is quite active and might generate the couple of void and electron under UV irradiation, some

generated void or electron cannot move to the particle surface and hence will not contact the aqueous solution. Therefore, the photocatalytic property of PVP capped ZnO nanoparticles was reduced. So, the photocatalytic degradation efficiencies of bare and PVP capped ZnO nanoparticles are entirely different under the same condition, and the photocatalytic activity of ZnO nanoparticles is greatly reduced after coating with PVP.

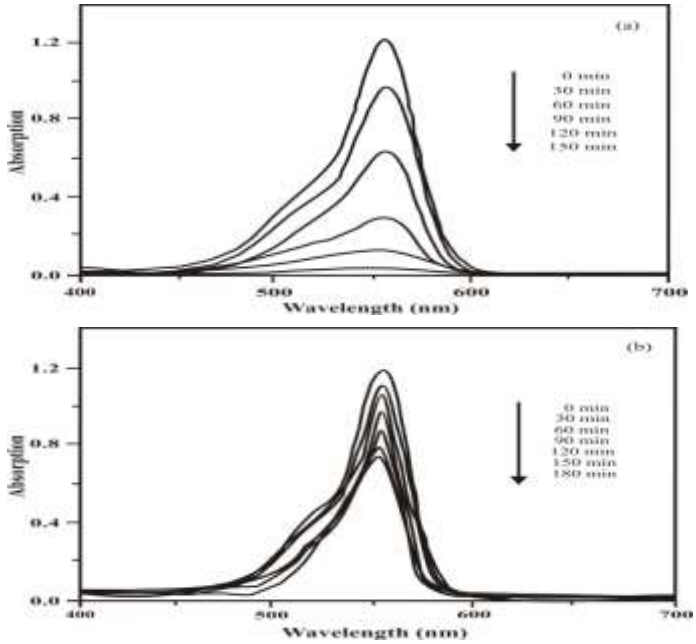

Fig.7. Absorption spectra of RhB solution as a function of UV light irradiation time in the presence of (a) bare and (b) PVP capped ZnO nanoparticles.

It can be seen that the suitable amount of PVP capping at most favorable catalysis conditions determined for the degradation of RhB using bare ZnO nanoparticles, is 250mg. The effect of concentration of PVP on the photodegradation of RhB using PVP capped ZnO nanoparticles are shown in Fig. 8. The photostability of RhB molecules can be improved by increasing the PVP concentration on the ZnO nanoparticles. The photodegradation efficiency of PVP capped ZnO nanoparticles decreased from with increasing the PVP concentration from 100mg to 250mg beyond which increasing the concentration of capping agent shows no noteworthy effect on the photodegradation efficiency of RhB. It may be attributed to the fact that as the capping agent concentration increases beyond the most favorable level it may decrease the dye adsorption, by covering some active sites. Hence an appropriate amount of capping agent helps to achieve a control over the photocatalytic activity of ZnO nanoparticles.

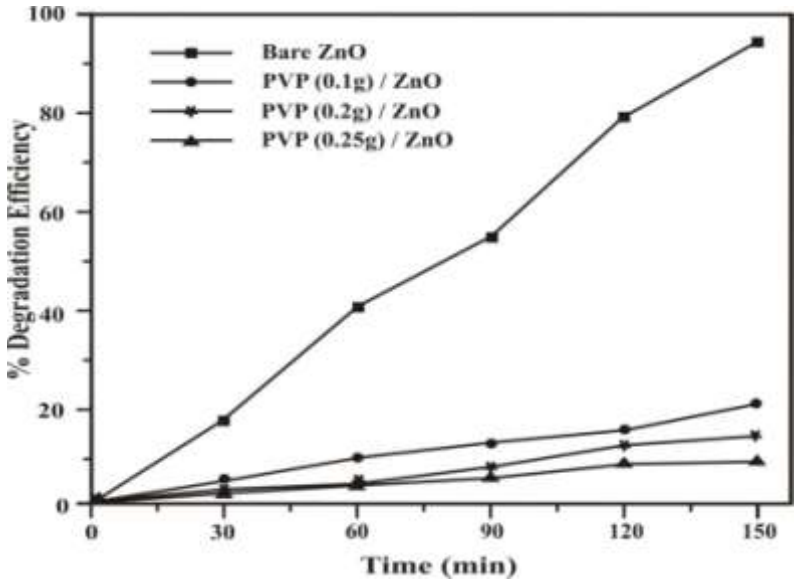

Fig.8. Percentage degradation efficiency of RhB using bare and PVP capped ZnO nanoparticles.

3.2.3. Chemical oxygen demand (COD)

The chemical oxygen demand test is widely used as an effective technique to measure the organic strength of waste water. The test allows the measurement of waste in terms of the total quantity of oxygen required for the oxidation of organic matter to CO_2 and water. In the present work results of COD were taken as one of the parameter to judge the feasibility of photocatalytic process for the degradation of RhB dye solution. The $K_2Cr_2O_7$ method was applied for COD determination and the treated solution showed a significant decrease in the COD value of the initial colour solution indicating the high potential of the bare ZnO nanoparticles catalyzed photodegradation process for the removal of RhB. Table. 1 gives the COD values of Initial and treated RhB solutions. The photodegradation efficiency is calculated from Eq. (1).

Maximum degradation efficiency was obtained for bare ZnO nanoparticles but RhB solution treated with PVP capped ZnO nanoparticles under similar conditions shows an average efficiency which indicates that the photocatalytic activity of PVP capped ZnO nanoparticles was reduced when compared with bare ZnO nanoparticles.

RhB Concentration (10^{-5} M)	**Initial COD (mg/L)**	**Final COD (mg/L)**		**Photodegradation efficiency (%)**	
		Bare ZnO	**PVP capped ZnO**	**Bare ZnO**	**PVP capped ZnO**
1	18.1	7.0	11.47	61.32	36.6
2	24.9	0	8.73	99.22	64.9
3	48.8	14.5	27.4	70.28	43.8
4	94.6	9.1	43.04	90.38	54.5
5	189.2	22.5	75.68	88.10	60.0

Table 1. COD values of initial and treated RhB solutions

3.2.4. Total organic carbon analysis

In order to further study the mineralization of RhB by the prepared bare and PVP capped ZnO nanoparticles, the TOC concentration of aqueous RhB solution at different reaction times was analyzed and the results were shown in Fig.9. The results show that RhB solution can be effectively mineralized to CO_2 and H_2O by the prepared bare ZnO nanoparticles under UV irradiation. In addition, it also can be seen that PVP capped ZnO nanoparticles showed poor mineralization efficiency compared with the bare ZnO nanoparticles. We proposed that this might be due to RhB molecules having different adsorption characters by the bare and PVP capped ZnO nanoparticles. The results above indicated that the bare ZnO shows good photocatalytic activity than the PVP capped ZnO nanoparticles.

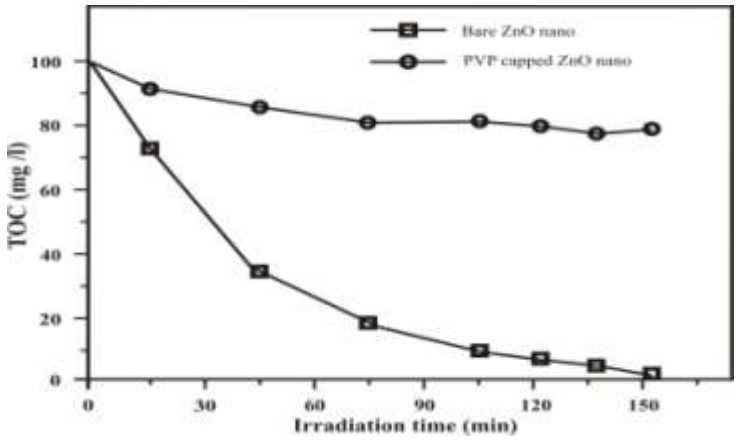

Fig.9. The effect of irradiation time on the photodegradation of RhB over bare ZnO and PVP capped ZnO nanoparticles.

3.3. UV shielding ability

The UV –Vis transmittance spectra of bare and PVP capped ZnO are presented in Fig.10. The transmittance spectra show an excellent UV-absorption capacity and high transparency in visible light for both bare and PVP capped ZnO nanoparticles. The transmittance spectrum also suggests that PVP capping do not influence the UV-shielding property and transparency in the visible light region of ZnO.

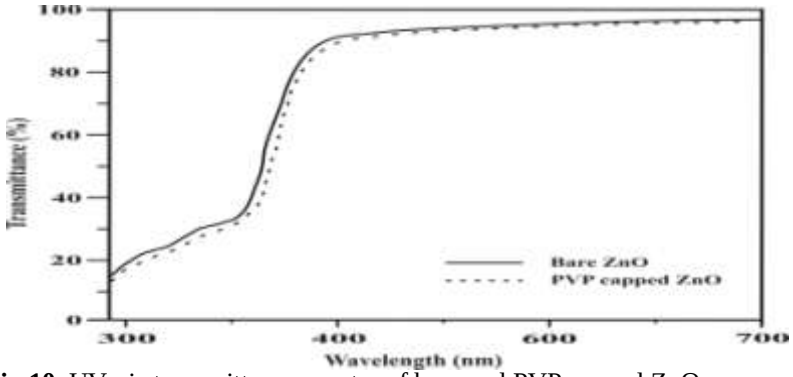

Fig.10. UV-vis transmittance spectra of bare and PVP capped ZnO nanoparticles.

IV. Conclusions

In this work bare and PVP capped ZnO nanoparticles were synthesized through precipitation method and their photocatalytic activity was evaluated by monitoring the photobleaching of the aqueous solutions of RhB dye under the irradiation of UV light. RhB photodegradation using bare and PVP capped ZnO nanoparticles as catalysts were observed through UV–visible spectroscopy which was found to be depend upon various parameters like catalyst dose, pH, initial concentration of dye and concentration of PVP. PVP capping markedly depressed the photocatalytic activity of ZnO nanoparticles and improves the photostability of RhB by acting as a barrier between ZnO and surrounding media to reduce the generation of O_2^- or $^{\cdot}OH$ species. The polymer capping not only prevents agglomeration of the nanoparticles but also minimized the photodegradation of RhB which has much needed the technological importance. This reduction in photocatalytic activity is important for ZnO nanoparticles to be used as UV shielding agents to protect organic substrates. These PVP/ZnO hybrid nanoparticles would significantly expand the applications of ZnO for the UV protection of a wide range of materials. The results obtained in this study demonstrate that the photocatalytic activity of ZnO nanoparticles can be optimized for different applications using different polymers as capping agents.

References

[1] T.D. Nguyen-Phan, V.H. Pham, T.V. Cuong, S.H. Hahn, E.J. Kim, J.S. Chung, S.H. Hur and E.W. Shin, *Mater. Lett*., **64,** 1387 (2010.
[2] Y.R. Zhang, J. Wan and Y.Q. Ke, *J. Hazard. Mater*., **177,** 750 (2010.
[3] N. Sobana and M. Swaminathan, *Sol. Energy Mater. Sol. Cells*., **91,** 727 (2007).
[4] J. Marto, P.S. Marcos, T. Trindade and J.A. Labrincha, *J. Hazard. Mater*., **163,** 36 (2009).
[5] L.Y. Yang, S.Y. Dong, J.H. Sun, J.L. Feng, Q.H. Wu and S.P. Sun, *J. Hazard. Mater*., **179**, 438 (2010.
[6] J.S. Xie and Q.S. Wu, *Mater. Lett*., **64,** 389 (2010).
[7] Z.L. Wang,, *Mater. Today*., **7,** 26 (2004).
[8] Y.Q. Li, S.Y. Fu and Y.W. Mai, *Polymer*., **47,** 2127 (2006).
[9] T. Iwasaki, M. Satoh, T. Masuda and T. Fujita, *J. Mater. Sci*., **35,** 4025 (2000).
[10] Z. Dang, L. Fan, S. Zhao and C. Nan, *Mater. Res. Bull*., **38,** 499 (2003).
[11] H. Usui, Y. Shimizu, T. Sasaki and N. Koshizaki, *J. Phys. Chem. B.*, **109** (2004).
[12] Y. Li, G. Li and Q. Yin, *Mater. Sci. Eng, B.,* **130,** 264 (2006).
[13] B. Baruwati, D.K. Kumar and S.V. Manorama, *Sens. Actuators B.*, **119,** 676 (2006).
[14] G.C. Yi, C. Wang and W.I. Park, *Semicond. Sci. Technol*., **20,** 22 (2005).
[15] Z.S. Wang, C.H. Huang, Y.Y. Huang, Y.J. Hou, P.H. Xie, B.W. Zhang and H.M. Cheng, *Chem. Mater*., **13,** 678 (2001).
[16] J. Zhou, N.S. Xu and Z.L. Wang, *Adv. Mater*., **18,** 2432 (2006).
[17] H.W. Engels, H.J. Weidenhaupt, M. Abele, M. Pieroth and W. Hofmann, in: *Ullmann's Encyclopedia of Industrial Chemistry*, sixth ed. (Electronic release: 2001).
[18] H. Heine, H.G. Vo¨ lz, J. Kischkewitz, P. Woditsch, A. Westhaus, W.-D. Griebler and M. de Liederkerke, in: *Ullmann's Encyclopedia of Industrial Chemistry*, sixth ed. (Electronic release: 2001).
[19] C.H. Yan, J. Zhang and L.D. Sun, in: H.S. Nalwa (Ed.), *Encyclopedia of Nanoscience and Nanotechnology*, American Science Publishers, **10**, 767 (2004).
[20] A. Becheri, M.Durr, P.L.Nostr and P. Balglioni , *J. Nanopart. Res*., **10 (4),** 679 (2008).
[21] R.H.Wang, J.H. Xin and X.M. Tao, *Inorg. Chem*., **44 (11),** 3926 (2005).
[22] A.C.Dodd, A.J.McKinley, M.Saunders and T.Tsuzuki, *J. Nanopart. Res*., **8 (1),** 43 (2006).
[23] B.Innes, T.Tsuzuki, H.Dawkins, J.Dunlop, G.Trotter, M. Nearn and P.G.McCormick, *Nanotechnology and the Cosmetic chemist, Nutracos Cosmet*., **1 (5),** 7 (2002).
[24] L.Sun, J.A.Rippon, P.G. Cookson, O. Koulaeva and R.Beltrame, *Int.J.Tech. Trans. Commerc*.,**7,** 224 (2008).
[25] L.Sun, J.A.Rippon, P.G. Cookson, O. Koulaeva and X.G.Wang, *Chem. Eng. J*., **147 (2-3),** 391(2009).
[26] R.Dunford, A.Salinaro, L.Cai, N.Serpone, S.Horikoshi, H.Hidaka and J.Knowland, *FEBS Lett*., **418 (1-2),** 87 (1997).
[27] B. Krishnan, L. Irimpan, V.P.N. Nampoor and V. Kumar, *Phys. E*., **40,** 2787 (2008).
[28] Y.L. Wu, A.I.Y. Tok, F.Y.C. Boey, X.T. Zeng and X.H. Zhang, *Appl. Surf. Sci*., **253,** 5473 (2007).
[29] L. Guo and S. Yang, *Chem. Mater*., **12,** 2268 (2000).
[30] R. Viswanatha, S. Sapra, B. Satpati, P.V. Satyam, B.N. Devb and D.D. Sarma, *J. Mater. Chem.*, **14,** 661 (2004).
[31] B. Krishnan, L. Irimpan, A. Deepthy, V.P.N. Nampoori and P. Radhakrishnan, *J. Phys. D: Appl. Phys*., **40,**5670 (2007).
[32] L. Guo, S. Yang,C. Yang, P. Yu, J. Wang, W. Ge, K. George and L. Wong, *Chem. Mater*., **12,** 2268 (2000).
[33] A. El Badawy, T. Luxton, R. G. Silva, K. G. Scheckel, M. T. Suidan and T. M. Tolaymat, , *Environ. Sci. Technol*., **44,** 1260 (2010).
[34] Chang Chun Chen, Ping Liu and ChunHua Lu, *Chem. Eng. J.*, **144,**509 (2008).